

We are IntechOpen, the world's leading publisher of Open Access books Built by scientists, for scientists

4,800

Open access books available

122,000

International authors and editors

135M

Downloads

Our authors are among the

154

Countries delivered to

TOP 1%

most cited scientists

12.2%

Contributors from top 500 universities



WEB OF SCIENCE™

Selection of our books indexed in the Book Citation Index
in Web of Science™ Core Collection (BKCI)

Interested in publishing with us?
Contact book.department@intechopen.com

Numbers displayed above are based on latest data collected.
For more information visit www.intechopen.com



Chapter

Estimation of Shear Wave Velocity Profiles Employing Genetic Algorithms and the Diffuse Field Approach on Microtremors Array: Implications on Liquefaction Hazard at Port of Spain, Trinidad

*Walter Salazar, Garth Mannette, Kafele Reddock
and Clevon Ash*

Abstract

This book chapter explains the methodology to determine the shear wave velocity V_s profile employing microtremors array data at Port of Spain, Trinidad, and its implication in the seismic amplification and liquefaction hazard in the city. We divide this study into five sections; firstly, we introduce a description of the spectral autocorrelation method and the genetic algorithm schemes to retrieve the V_s and thickness of soil layers. Secondly, we validate the soil profiles via inspection of the ellipticity pattern at such sites; we also compared the observed horizontal-to-vertical spectral ratios (H/V) with the synthetic ones derived by the Diffuse Field Approach and 1D theoretical SH wave amplification functions. Thirdly, we compute the shear wave velocity in the first 30 m obtained from our genetic inversion and compared with the ones estimated by the empirical formulas based on geomorphological conditions. Fourthly, we present a preliminary liquefaction hazard map based on the level of H/V microtremor ratios and the fundamental period of vibration. Finally, we conclude with further recommendations for planning purposes in the city of Port of Spain.

Keywords: shear wave velocity, genetic algorithms, fundamental period, liquefaction

1. Methods and data

1.1 Array measurement of microtremors

Port of Spain (POS) lies on an alluvial fan deposit and forms a costal aquifer with a high water table comprising poorly sorted gravels, sand, clay, and boulders. The part of today's downtown Port of Spain closest to the sea was once an area of tidal mudflats covered by mangroves which have been reclaimed by anthropological

means. Recent studies suggested a peak ground acceleration of about 0.6 g on rock sites for a 2475 year return period in POS. Salazar et al. [1] presented a high-resolution grid of H/V spectral ratios employing 1181 mobile microtremors at Port of Spain in order to retrieve the S-wave fundamental periods of vibration of the soil and proposed a microzonation map for the city and the correspondent seismic coefficients for building design. So the main objective of this article is to validate such periods through an alternative geophysical method, namely, the microtremors array, and use them to develop a liquefaction hazard map for the city based on the same H/V spectral ratios of microtremors.

Nine microtremors array were done at nine sites in POS located on recent alluvium and reclaimed land (**Figure 1**). The objective of the microtremors array is to obtain the shear wave velocity (V_S) profile at the site by locating seven sensors that measure vertical ambient vibrations in a circular configuration (see **Figure 2** and **Table 1**). Then the main idea of deploying an array is to compare the motion of sensor (1) located in the center of the circle with the motion on sensors (2–4) separated by a distance equal to the radii “r” of the circle located in the vertexes of the triangle. Through the comparison of the vertical motion that comprises Rayleigh waves, it is possible to work backward retrieving the V_S and thickness of the soil and bedrock layers through genetic inversions. So, with the V_S profiles, it is possible to obtain the soil amplification factors to be incorporated in seismic codes for building design.

To perform the microtremors array, we use a Tokyo Sokushin 9-channel SAMTAC 802-H and the sensors VSE-15D6 with a flat response between 0.1 and 100 Hz and a 24-bit recording system of $\Delta t = 0.01$ s equivalent to 100 samples per second; the sensors measured micromotion in terms of velocity (**Figure 3**). We recorded a total of 25 min for each array in a silent environment.

Since we had a recorder with nine channels, we locate in location number 1 three channels corresponding to two horizontal and one vertical component to compute

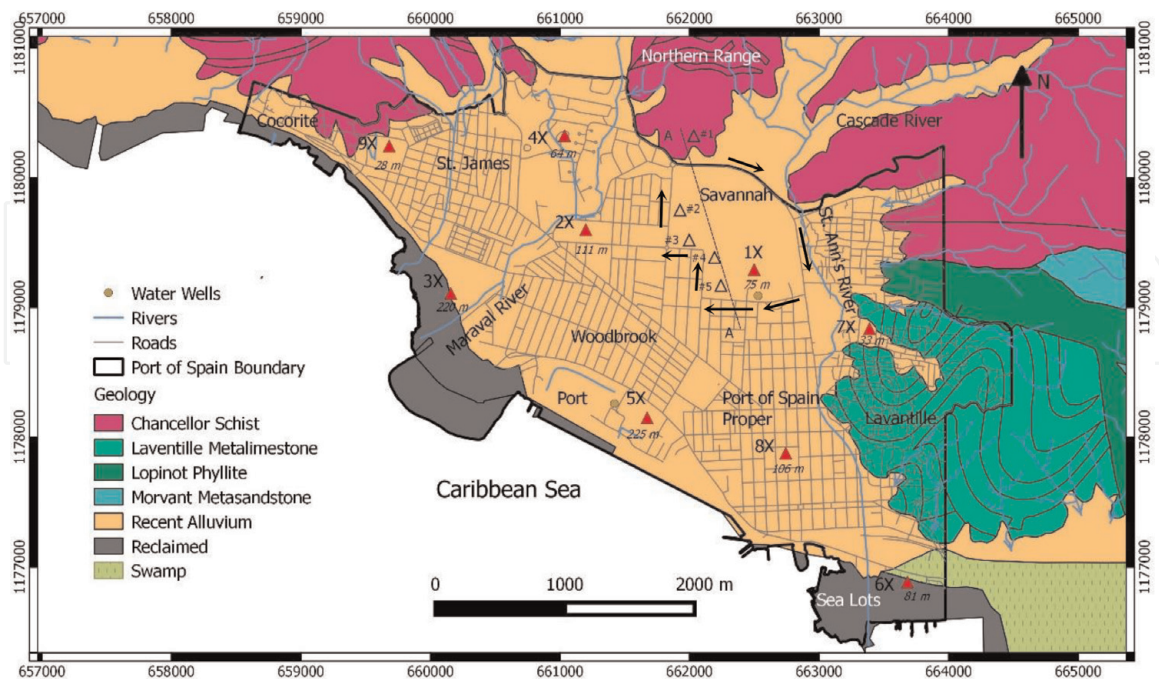


Figure 1. Geological map of Port of Spain. The locations of the nine microtremors array are depicted by a red solid triangle and a number with an X (e.g., 1X–9X, see **Table 1**); the corresponding thickness of sediments above the bedrock retrieved from the genetic inversions is depicted in cursive numbers. Water well data near the arrays are depicted with a solid brown circles (see thickness and soil layers classification in **Figure 6** and **Table 5**); open triangles denote boreholes reaching the bedrock; see elevation model of section A–A in **Figure 6**. Arrows in the clockwise direction around the Queen’s Park Savannah indicate the flow of constant traffic in the roundabout of 500 m radii.

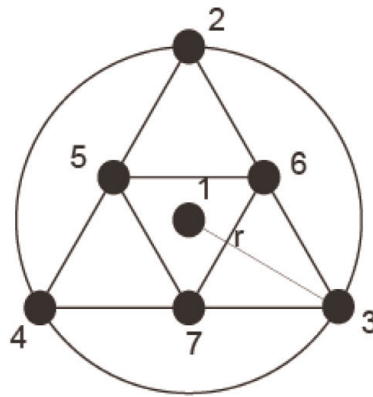


Figure 2.

Top: general microtremors array configuration in a plan view. The sensors 1, 2, 3, and 4 represent the array with the largest radii r , while the sensors 5, 6, and 7 represent the array with the smallest radii $r/2$. Since we had a recorder of nine channels, we set in location number 1 three channels corresponding to two horizontal and one vertical component, while the remaining numbers (2–7) we locate just one vertical sensor. Bottom: photo of an array at Mucurapo Secondary School (site 3X in Figure 1).

the H/V spectral ratios [4], while in the remaining location numbers (2–7), we locate just one vertical sensor.

1.2 Spectral autocorrelation (SPAC) and dispersion curve

The comparison of the recorded vertical motion is made in the frequency domain via application of the spatial autocorrelation method (SPAC) [5, 6]. The first step in the SPAC method is to compute the cross spectra S_{ij} through Fourier transformation of the signal, and then the autocorrelation function R_{ij} of the sensor $j = (2, 3, 4)$ in the vertex of the triangle with central site 1 yields as follows:

$$R_{ij}(f) = \frac{S_{ij}(f)}{[S_{11}(f)S_{jj}(f)]^{0.5}} \quad (1)$$

where f denotes frequency domain.

Array number	Location	Size of the array (radii r)		Maximum wavelength λ (m)	λ/\max array size
		Large circle	Small circle		
1X	Queen's Park Savannah	40 m (first) 10 m (second)	20 m (first) 5 m (second)	393	9.8
2X	Nelson Mandela Park	40 m (first) 10 m (second)	20 m (first) 5 m (second)	379	9.5
3X	Mucurapo Secondary School	40 m (first) 10 m (second)	20 m (first) 5 m (second)	447	11.2
4X	Federation Park	20 m (first) 5 m (second)	10 m (first) 2.5 m (second)	280	14
5X	Port Area (Licensing Authority)	40 m (first) 10 m (second)	20 m (first) 5 m (second)	570	14.3
6X	Sea Lots	40 m (first) 10 m (second)	20 m (first) 5 m (second)	213	5.3
7X	St. Dominic's Children's Home	20 m (first) 5 m (second)	10 m (first) 2.5 m (second)	77	3.9
8X	Woodford Square	40 m (first) 10 m (second)	20 m (first) 5 m (second)	248	6.2
9X	St. James Hospital	20 m (first) 5 m (second)	10 m (first) 2.5 m (second)	117	5.9

See general plan view and photo of an array in **Figure 2**. Maximum wavelength is calculated from dispersion curves on **Figures 5 and 7** as $\lambda = c_o/f$, where c_o is the phase velocity and f denotes frequency in Hz.

Table 1.

Selected sites for the microtremors array in Port of Spain (see location in **Figure 1**).

Then the direction average of the autocorrelation function ρ (SPAC) for the three sensors separated by a radii r gives:

$$\rho(f,r) = \frac{1}{3} \sum_{j=2}^4 R_{1j}(f,r) \quad (2)$$

The vertical motion is also compared with sensor (1) and sensors (5–7) which corresponds to a radius equal to “ $r/2$ ” (**Figure 2**). We used several aperture

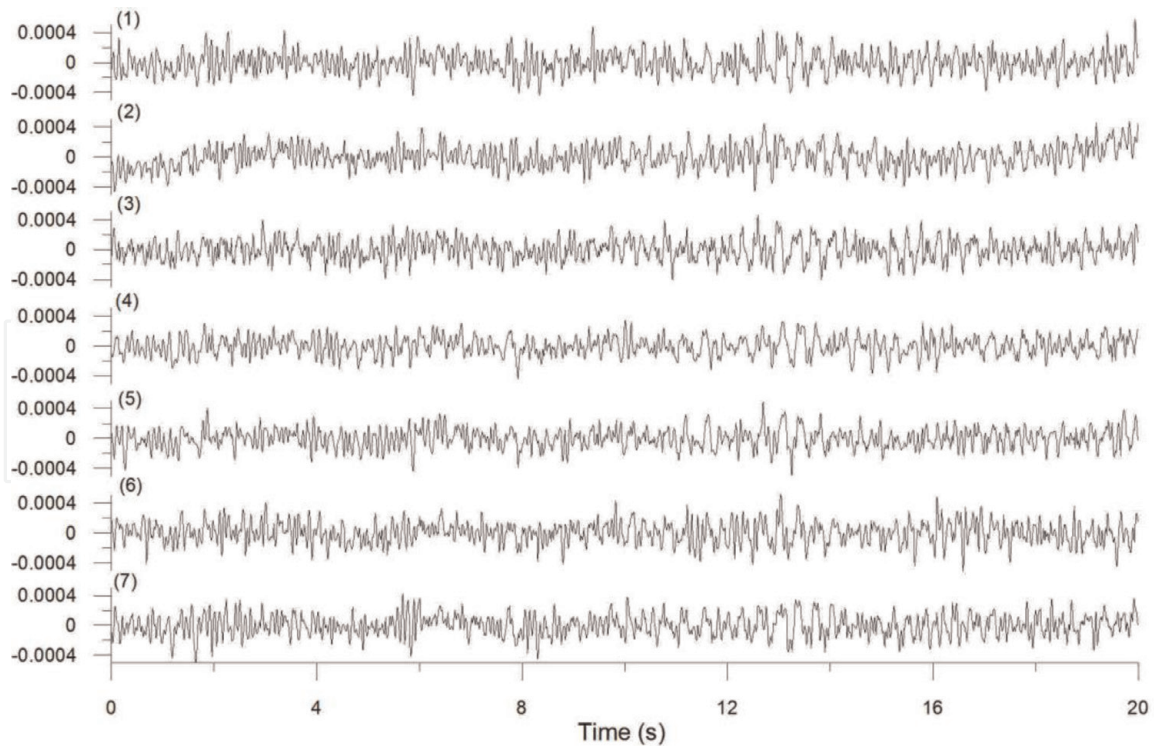


Figure 3. Example of velocity history (cm/s) for the vertical component of the microtremors array in Mucurapo Secondary School. See the number of channel in the left upper part of each record in accordance to the array configuration in **Figure 2**. Channel 1 corresponds to the sensor located in the center; sensors 2, 3, and 4 correspond to the radii of 40 m and sensors 5, 6, and 7 to the radii of 20 m in the vertices of the triangles.

maximum radii between 20 and 40 m depending on the available space at the site of interest, and we repeat the procedure for a small array that corresponds to $r/4$ and $r/8$.

We present the results of the SPAC at the Queen's Park Savannah array (site 1X in **Figure 1**), for the radii of 5, 10, 20, and 40 m (**Figure 4**); we calculated the average of the SPAC for 81.92 s of stationary parts of the signal. The SPAC with values of about +1.0 means that the wave motion at short frequencies is very similar regardless of the aperture of the array, and the SPAC decreases as the frequency increases; the negative value in the SPAC represents change of polarity in the wave motion for longer frequencies (shorter periods).

To obtain the observed Rayleigh wave velocity $c_o(f)$, a 0-order Bessel function of first kind $J_0(x)$ is used as follows:

$$\rho(f, r) = J_0(x) = J_0\left(\frac{2\pi fr}{c_o(f)}\right) \quad (3)$$

Employing the argument x of the Bessel function, the phase velocity yields:

$$c_o(f) = \frac{2\pi fr}{x} \quad (4)$$

Figure 5 shows the resulting dispersion curve (phase velocity) for the Queen's Park Savannah array through the SPAC employing a 0-order Bessel function of first kind. To get a single dispersion curve, we averaged the four common parts of each phase velocity from the different array sizes and added the single reliable parts of the dispersion curves corresponding to the maximum and minimum array sizes. Arrays with a bigger aperture are able to retrieve the velocities for low frequencies (long period) of motion and subsequently retrieve a deeper soil structure; arrays with smaller aperture are able to retrieve the velocities for high frequencies (shorter

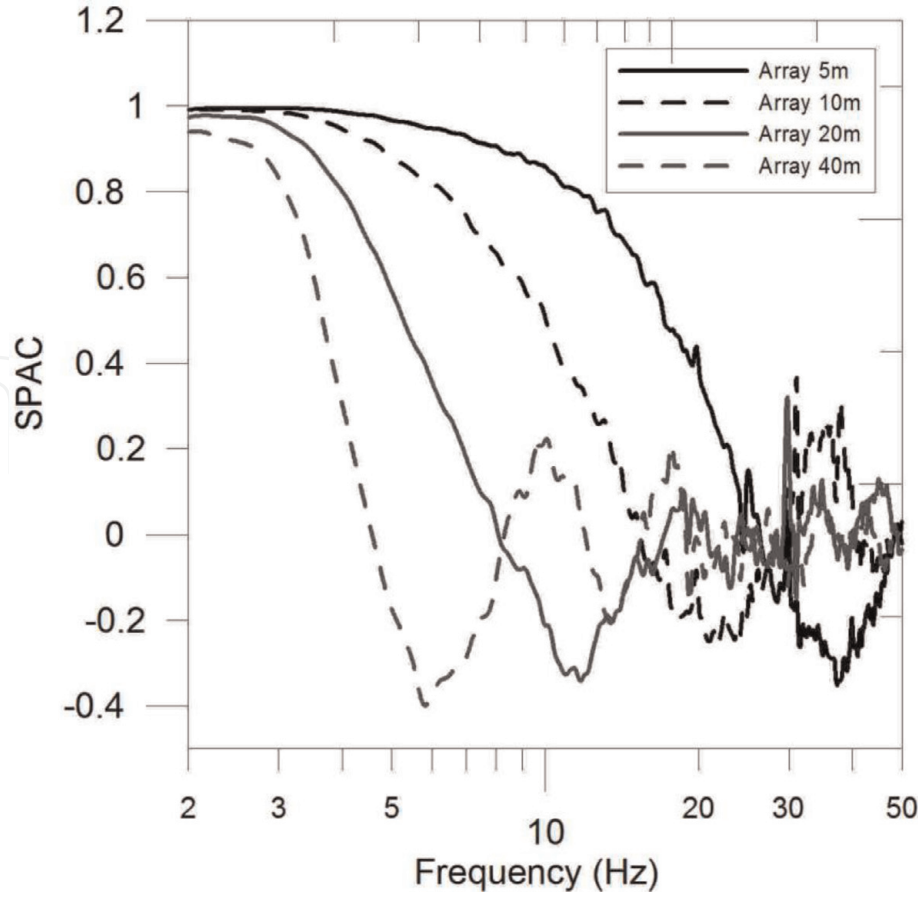


Figure 4. Spatial autocorrelation coefficient (SPAC) for the Queen’s Park Savannah array of microtremors (point 1X in Figure 1).

period) with a better resolution for soil structures near the surface. Note that each phase velocity in the arrays has unreliable parts for very low- and high-frequency components of motion due to the aperture radii used in each case; in other words, an array has a limited frequency band of usefulness between f_{min} and f_{max} that is dependent on its aperture. Rayleigh waves are dispersive and their velocities decrease with frequency; the reliable parts of each phase velocity must follow such trend eliminating in the average calculation the increase of velocity at low and high frequencies of motion. We noticed that the maximum wavelength at which the phase velocity can be estimated is about 10 times the radii r of the arrays at Queen’s Park Savannah (Figure 5); the minimum wavelength is about 2 times the radii r of the arrays [7]. To obtain the average velocity at each frequency of motion f , we used N frequencies equally separated by the value of Δ_f in terms of a logarithm scale as follows:

$$\log \Delta_f = \frac{\log f_{max} - \log f_{min}}{N - 1} \quad (5)$$

where f_{max} and f_{min} are the maximum and minimum reliable frequencies for the aperture arrays, respectively (Figure 5). In our case, we generally set the value of $N = 20$ and select the corresponding velocity which belongs to the nearest frequency in such interval.

1.3 Inversion of phase velocities through genetic algorithms (GAs)

Genetic algorithms (GAs) are mathematical simulations based on biological evolution of natural selection rules. The soil parameters are digitized to gene type

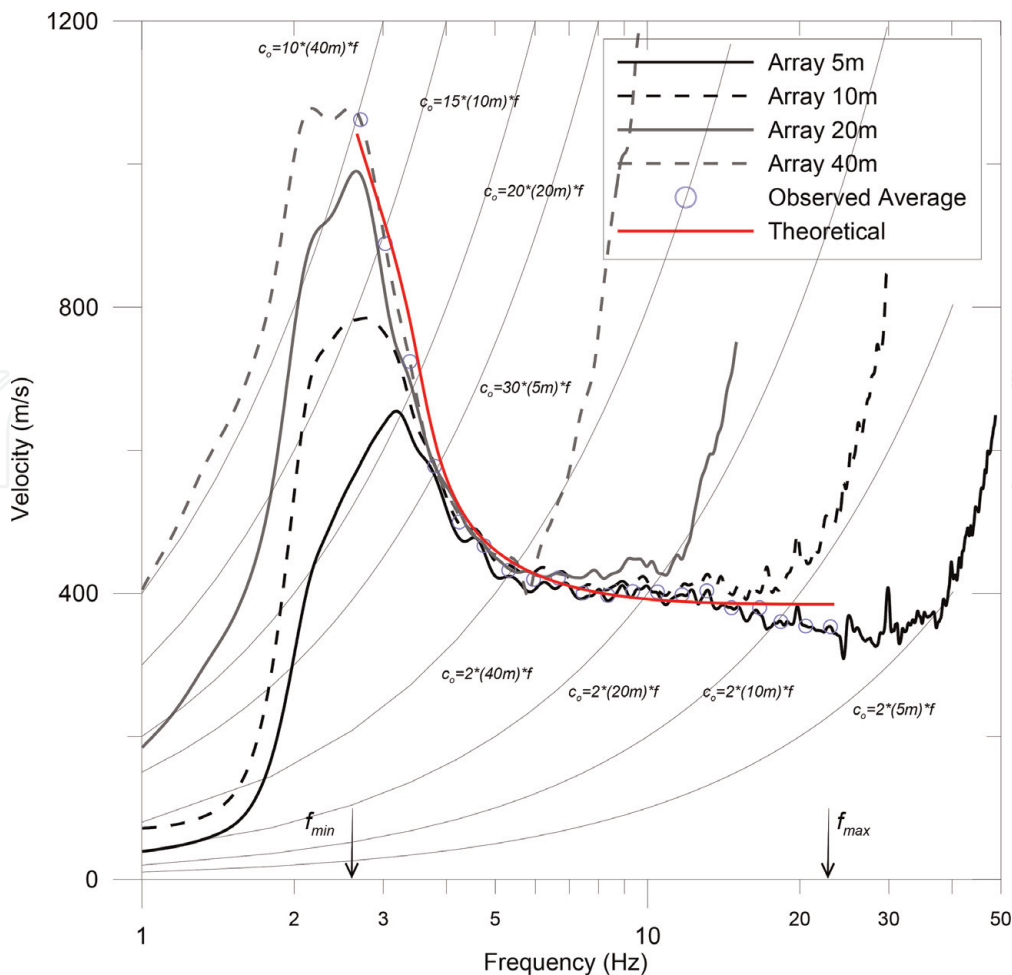


Figure 5. Dispersion curve of Rayleigh wave (phase velocity) for Queen's Park Savannah array (point 1X in Figure 1). We select the average velocity (open circles) of the four radii r to be used in the genetic inversion. The thin solid lines depict the wavelength that corresponds to 10–30 times and 2 times the radii of the arrays. The red thick solid line depicts the theoretical phase velocity curve that corresponds to best individual (soil profile in Figure 6) after searching the optimum solution via genetic algorithms; f_{max} and f_{min} are the maximum and minimum reliable frequencies for the aperture arrays.

with n bits in series of 0 and 1 defining a priori lower and upper bound limits for the shear wave velocity and thickness of the layer (e.g., 200–600 m/s and 10–100 m, respectively). Each bit represents a gene, and a series of bits concatenated represents a chromosome. So, an optimal solution is searched using the chromosome that best matches the soil model represented by the experimental phase velocity curve developed using the microtremors array after applying the SPAC method. In this work we employed the method of Yamanaka and Ishida [8]. The reproduction of the initial population to a new population relies on the fitness function of each individual applying the three genetic operations modulated by the selection, crossover, and mutation; crossover acts to generate a good, new model with the combination of good parts of chromosomes of two parents; in the mutation operation, a gene is reversed (e.g., from 1 to 0 or vice versa). The mutation procedure is necessary to escape trapping at local minimum solutions.

The selection process begins declaring a misfit function ϕ_k for a k individual is defined as follows:

$$\phi_k = \frac{1}{N} \sum_{i=1}^N \left[\frac{c_o(f) - c_c(f)}{\sigma_c(f)} \right]^2 \quad (6)$$

where N is the number of observed data that correspond to the number of the discrete frequencies used in the analysis (see Eq. (5)), $c_o(f)$ is the observed Rayleigh wave velocity retrieved from the SPAC, $c_c(f)$ is the calculated Rayleigh wave velocity, and σ_c is the standard deviation of the calculated velocity based on the average of all n individuals that constitute a population. Note that $c_c(f)$ is obtained theoretically employing the Haskell [9] model for plane waves using the V_S and the thickness of layers produced by the genetic reproduction.

Then a fitness function fit is based on the misfit function as follows:

$$fit_k = \frac{1}{\phi_k} \quad (7)$$

In the inversion, the soil model that fits the observed data must have a high value of fitness and survives to a greater extent to the next generation, while the models with a low value of fitness (bad ones) are replaced by newly generated models.

It is noted that some authors (e.g., [10]) suggest that the dispersion curve is not carrying information (or very limited) of the velocity and the position of the bedrock; in such cases both parameters are badly constrained if we set a broad lower and upper bound of V_S for the half space in the bedrock during one round of a GAs' process. According to the seismic refraction data for the region [11], the bedrock yields a V_S of 2000 m/s. However, such V_S value was obtained for the Cariaco sedimentary basin at north eastern Venezuela which is located 225 km away from POS. In order to validate the V_S of 2000 m/s proposed by Schmitz et al. [11], we extended the original GAs employing successive rounds of inversions.

1.4 Successive rounds of genetic inversion

We applied successive rounds of GAs for the array at Queen's Park Savannah and St. Dominic's Children's Home (see site 1X and 7X, **Figure 1**) due to the following reasons:

- a. In the Queen's Park Savanna, there is water well information (see **Figure 6**) to compare with the genetic inversion results. The array site is also located inside of a busy roundabout of 500 m radii, so presumably the constant source of the energy of microtremors is guaranteed in this case due to constant traffic activity in clockwise direction (see arrows in **Figure 1**).
- b. St. Dominic's Children's Home has the shortest period among the array sites, and it is located 500 m from the roundabout (**Figure 1**). So it would be easy to get a reliable shear wave velocity on bedrock according to the aperture array size and a very shallow structure (**Table 1**).
- c. We want to compare the results of (a) and (b).

Then, the procedure for the successive genetic inversions for the Queen's Park Savannah site is as follows:

- a. We perform the first round of GAs with broad lower and upper bound limits for both, the soil deposits and the bedrock, namely, $V_s = 100\text{--}600$, $200\text{--}700$, and $300\text{--}800$ m/s for the first, second, and third layer, respectively, and thickness $H = 5\text{--}50$ m for all soil layers, and a $V_s = 1000\text{--}2200$ m/s for the bedrock (**Table 2**). The P-wave velocity was calculated from the S-wave velocity using empirical relation determined by Kitsunezaki et al. [12]. Generally, we assume

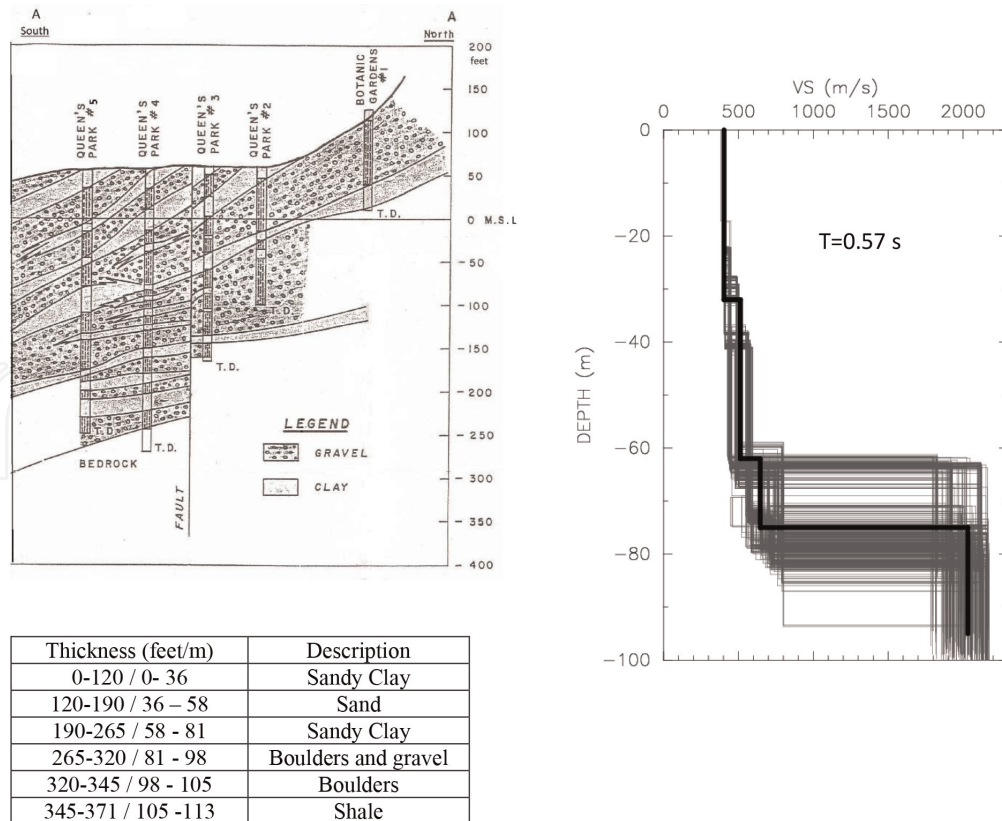


Figure 6. Left: boreholes at Queen’s Park Savannah. TD, terminal depth; MSL, mean sea level. Note that the total depth of the boreholes must be accounted above and below the MSL (e.g., depth $\approx 210 + 50 = 260$ feet or 80 m). Cross section A-A is located in **Figure 1** depicting boreholes reaching the bedrock in the Queen’s Park Savannah (after [2]). Right: Shear wave velocity profile obtained via genetic inversion of phase velocity at Queen’s Park Savanna (point 1X in **Figure 1**). The best model (thick black line) is considered the average for good models that fits into the 10% of average misfit (thin gray lines) in the final round of successive genetic inversions (**Table 2**). T denotes the fundamental period of the soil.

that the stiffness of soil increases with the depth, with an overlap in the V_S ranges between two consecutive soil layers to take into account the possibility of velocity reversal when increasing depth. The best model is considered the average for all models that fits into the 10% of average misfit, so we were able to calculate the standard deviation σ for the V_S and thickness H of each layer.

- b. We perform a second round of GAs selecting a narrow lower and upper bound limits for V_S for the bedrock from step (a) as the mean \pm standard deviation σ (e.g., 1705 ± 116); instead we select a broad lower and upper bound during the genetic reproduction of shear wave velocity and thickness of soil layers as shown in **Table 2** ($V_S = 100\text{--}600, 200\text{--}700,$ and $300\text{--}800$ m/s for the first, second, and third layer, respectively, and thickness $H = 5\text{--}50$ m for all layers).
- c. We perform a third round of genetic inversion fixing the V_S and thickness of the soil layers within the mean \pm standard deviation σ calculated in (b) and select broad lower and upper bound limits for the V_S of bedrock half space (**Table 2**), namely, $1000\text{--}2200$ m/s. Then a new value of V_S and its standard deviation for the bedrock are estimated in this step.
- d. We perform again step (b) with a new narrow lower and upper bound limits for V_S for the bedrock $\pm \sigma$ of the mean of step (c) and selecting again, a broad lower and upper bounds of V_S and thickness of soil layers.

Round	Search Limits			Final Optimal Model	
	Vs(m/s)	Thickness H (m)	Density $\rho(\text{g/cm}^3)$	Vs(m/s) $\pm \sigma$	H (m) $\pm \sigma$
1	100-600	5-50	1.6	346 \pm 3	9 \pm 0.3
	200-700	5-50	1.7	440 \pm 2	44 \pm 0.4
	300-800	5-50	1.8	682 \pm 11	27 \pm 0.7
	1000-2200	α	2.4	1705 \pm 116	α
2	100-600	5-50	1.6	390 \pm 5	18 \pm 2
	200-700	5-50	1.7	446 \pm 6	17 \pm 4
	300-800	5-50	1.8	464 \pm 46	31 \pm 2
	1589-1821	α	2.4	1752 \pm 50	α
3	385-395	16-20	1.6	389 \pm 3	17 \pm 0.6
	440-452	13-21	1.7	447 \pm 3	19 \pm 1
	418-510	29-33	1.8	464 \pm 9	31 \pm 1
	1000-2200	α	2.4	1899 \pm 208	α
4	100-600	5-50	1.6	405 \pm 6	31 \pm 9
	200-700	5-50	1.7	501 \pm 71	19 \pm 5
	300-800	5-50	1.8	532 \pm 114	22 \pm 7
	1691-2107	α	2.4	1928 \pm 107	α
5	399-411	22-40	1.6	402 \pm 3	29 \pm 3
	430-572	14-24	1.7	477 \pm 17	22 \pm 2
	418-646	15-29	1.8	513 \pm 29	20 \pm 3
	1000-2200	α	2.4	1979 \pm 193	α
6	100-600	5-50	1.6	403 \pm 5	32 \pm 7
	200-700	5-50	1.7	513 \pm 52	30 \pm 8
	300-800	5-50	1.8	645 \pm 126	13 \pm 7
	1786-2172	α	2.4	2032 \pm 104	α

σ denotes the standard deviation and α denotes infinite thickness on half space. The arrows indicate the bedrock or sediments information that is used in the subsequent round of GAs.

Table 2. Example of successive rounds of genetic inversion, search limits, and optimal final model for Queen’s Park Savannah site 1X.

- e. The schemes (b–d) is repeated till when we find the mean V_s for the soil deposits and bedrock inside of the range V_s mean $\pm \sigma$ of a previous round when selecting a narrow lower and upper bound in the bedrock (e.g., rounds 4 and 6 in **Table 2**).

Then the successive rounds of inversion are based on the effect of fixing the bedrock properties while searching the optimum solutions in one round of GAs

employing broad lower and upper bound limits for the sediments and vice versa through several rounds of inversions in a subsequent manner.

When applying the methodology above to the Queen's Savannah Park array, for each iteration, the total number of unknown parameters yields four velocities and three thicknesses, searching an optimal combination for them in the inversion that matches the experimental phase velocity presented in **Figure 5**. These parameters were digitized as 8-bit binary strings, setting the population size at $n = 30$ individuals, with a crossover probability of 0.7 and an initial mutation probability of 0.01, terminating the iterations at the 100th generation. Since the algorithm used initial random numbers finding the global minimum solution, we performed for each round of GAs 5 iterations (or inversions) that indeed had different initial random numbers with a total of 15,000 soil models in each round. The final model was selected as an acceptable solution if its average misfit was less than 10% [13, 14].

The GAs' inversion yields a value of $V_S = 2032 \pm 104$ m/s for the bedrock for the sixth round according to (e) above, which is basically the same value of 2000 m/s proposed by Schmitz et al. [11]. The results also yielded a first layer of $V_S = 403$ m/s with a thickness of 32 m, a second layer of $V_S = 513$ m/s with a thickness of 30 m, and a third layer of $V_S = 645$ m/s with a thickness of 12 m that are classified as sand and clay. The soil profile is presented in **Figure 6**. Then the total thickness yields 75 m above a half space constituted by a shear wave velocity of nearly 2000 m/s. We validated our results with the depth of bedrock of about 80 m (260 feet in **Figure 6**) in this area reported by the Water and Sewerage Authority (WASA) [2]. Note that the thickness of 32 ± 7 m of the first layer is similar to the sandy-clay first layer of 36 m with the water well profile presented in **Figure 6**; however, some differences are found to the second and third layer. We attribute such differences due to the fact that such water well information is 200 m apart from the array site. The bedrock in this case is found at the boulders' level.

It is noted a good match between the experimental and calculated (theoretical) phase velocity via application of the Haskell [9] model for plane waves employing the final model presented in **Table 2**. This confirms the effectiveness of the genetic scheme (**Figure 5**).

The authors tested secondly the successive rounds of GAs performing an array at St. Dominic's Children's Home (see site 7X, **Figure 1**) with the shortest period of 0.22 s among the arrays (see **Figure 10h**). Then it would be suitable to find the V_S for the bedrock for a shallower and a simple soil structure. The results are presented in **Table 3**.

It is noted that we found also a value near 2000 m/s for the bedrock when applying the GAs at this site. As it was expected, for the St. Dominic's Children's Home case, the GAs converge faster than for the Queen's Park Savannah case due to a simple and shallower soil structure.

If we fix the V_S for the bedrock as $V_S 2032 \pm 104$ m/s taken from round number six in **Table 2** from GAs in Queen's Park Savannah and perform one round of GAs for St. Dominic's Children's Home, we found practically the same optimal model for the soil profile from the previous process above (**Table 4**).

Further seven microtremors array were made in Port of Spain and distributed in the City (**Figure 1** and **Table 1**); for such cases we fix in the GAs' scheme the $V_S 2008 \pm 124$ m/s in the half space according to round 4 in **Table 3**. The proportion of the maximum wave length and the array size lay between 4 and 14 for all measurements (see **Table 1**). So we assured that the search limits for the thickness of the soil deposits in the GAs' process yield less than the penetration of the Rayleigh waves for each array. A commonly adopted criterion is that the maximum investigation depth is half of the maximum wavelength [15]. Appropriate search limits were decided after several trial runs. The results of the GAs' inversion are

Round	Search Limits			Final Optimal Model	
	Vs(m/s)	Thickness H (m)	Density $\rho(\text{g/cm}^3)$	Vs(m/s) $\pm \sigma$	H (m) $\pm \sigma$
1	100-600	5-50	1.6	285 \pm 1	9 \pm 0.03
	300-800	5-50	1.8	552 \pm 2	24 \pm 0.9
	1000-2200	α	2.4	1948 \pm 200	α
2	100-600	5-50	1.6	284 \pm 2	9 \pm 0.04
	300-800	5-50	1.8	552 \pm 2	24 \pm 0.8
	1748-2148	α	2.4	2045 \pm 93	α
3	282-286	8-10	1.6	284 \pm 0.5	9 \pm 0.1
	550-554	23-25	1.8	551 \pm 1	24 \pm 0.5
	1000-2200	α	2.4	1931 \pm 239	α
4	100-600	5-50	1.6	284 \pm 2	9 \pm 0
	300-800	5-50	1.8	552 \pm 2	24 \pm 0.7
	1692-2170	α	2.4	2008 \pm 124	α

σ denotes the standard deviation and α denotes infinite thickness on half space. The arrows indicate the bedrock or sediments information that is used in the subsequent round of GAs.

Table 3.

Example of successive genetic inversion, search limits, and optimal final model for St. Dominic's Children's Home site 7X.

Round	Search Limits			Final Optimal Model	
	Vs(m/s)	Thickness H (m)	Density $\rho(\text{g/cm}^3)$	Vs(m/s) $\pm \sigma$	H (m) $\pm \sigma$
1	100-600	5-50	1.6	285 \pm 2	9 \pm 0.04
	300-800	5-50	1.8	553 \pm 2	24 \pm 0.4
	1928-2136	α	2.4	2047 \pm 34	α

σ denotes the standard deviation and α denotes infinite thickness on half space. We fix the bedrock velocity according to the results of the Successive Inversion for Queen's Park Savannah (Table 2).

Table 4.

Example of genetic inversion, search limits, and optimal final model for St. Dominic's Children's Home site 7X.

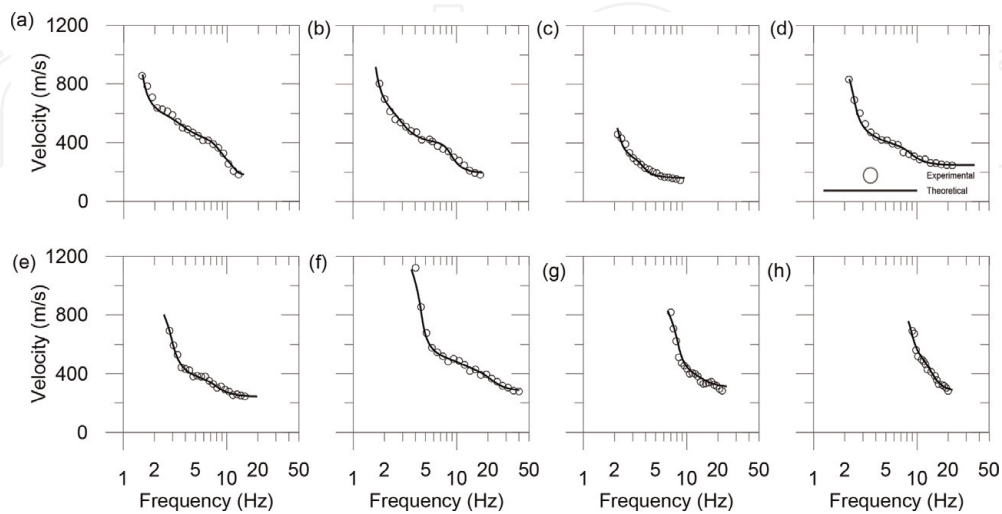


Figure 7.

Theoretical (line) and experimental (open circles) phase profiles after application of the genetic inversion at eight sites of microtremors array in Port of Spain. (a) Port Area (5X), (b) Mucurapo Secondary School (3X), (c) Sea Lots (8X), (d) Nelson Mandela Park (2X), (e) Woodford Park (8X), (f) Federation Park (4X), (g) St. James hospital (9X), and (h) St. Dominic's Children's home (7X). See locations of microtremors array in Figure 1.

presented in **Figures 7** and **8**. It is observed a good match between the experimental and calculated (theoretical) phase velocity for all array sites. The soil profiles containing the V_S and thickness resulting from the microtremors array analysis are plotted in **Figure 8**. The shear wave velocity in the POS sediments yields from 51 to 750 m/s and the bedrock is located at 28 to 225 m depth with shallow structures in the peripheries near the hills and deeper structures toward the south of the city at the Port Area (**Figure 1**). It is worth mentioning that at the Port Area, very

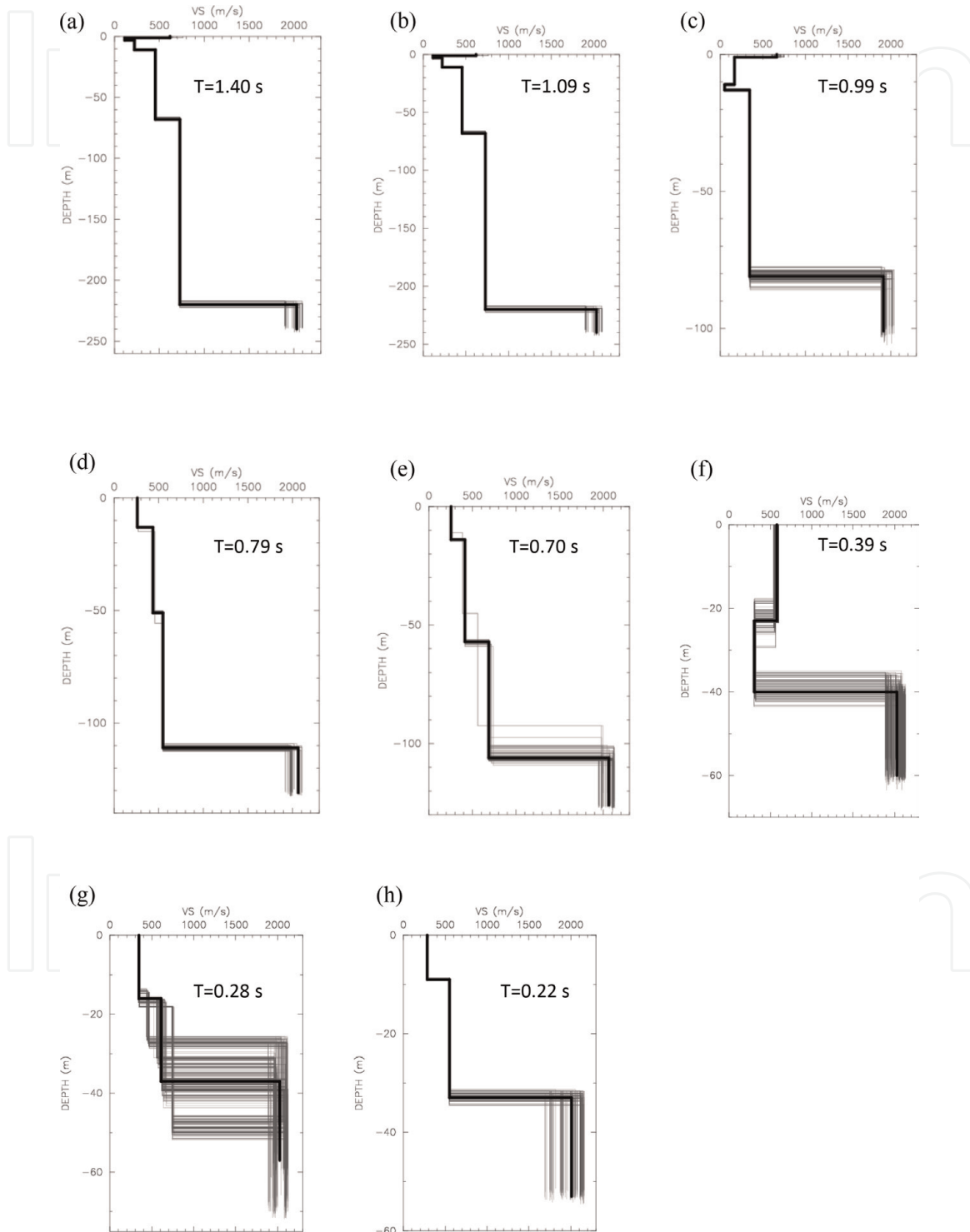


Figure 8. Mean shear wave velocity (V_S) profiles after application of the genetic inversion at eight sites of microtremors array in Port of Spain. The best model (thick black line) is considered the average for good models that fits into the 10% of average misfit (thin gray lines). (a) Port Area (5X), (b) Mucurapo Secondary School (3X), (c) Sea Lots (8X), (d) Nelson Mandela Park (2X), (e) Woodford Square (8X), (f) Federation Park (4X), (g) St. James hospital (9X), and (h) St. Benedict's Children's home (7X). The sites are ordered from top to bottom from the largest to the shortest fundamental period of soil T (s). See locations of microtremors array in **Figure 1**.

consolidated sediments with V_S of about 700 m/s constitute the thicker layers with more than 100 m above the bedrock.

2. Results and discussion

2.1 H/V interpretations: the Diffuse Field Approach and the ellipticity of Rayleigh waves

Despite some authors have performed a joint inversion of the phase velocity and the H/V observed spectral ratios [16], we preferred to validate our V_S profile retrieved from the GAs generating synthetics' H/V ratios via application of the Diffuse Field Approach (DFA) and compare them with the observed ones. If we incorporate the observed H/V curve in a joint inversion, we would force a priori the soil profiles to fit with such curve, issue that the new interpretation of DFA would validate completely in a separate manner.

The soil profiles' results by the GAs' inversion of the previous section are validated via two alternative analyses: (i) the theoretical H/V ratios inferred from the Diffuse Field Approach (DFA) and the observed H/V ratios; (ii) the theoretical H/V ellipticity of Rayleigh waves.

Recently a new interpretation has been proposed and formulated by Sánchez-Sesma et al. [17, 18] and Pertou et al. [19] based on a Diffuse Field Approach that the H/V ratios on microtremors can be interpreted as the square root of the ratio of the sum of horizontal displacements for horizontal unit harmonic loads $\text{Im}[G_{11}]$ and $\text{Im}[G_{22}]$ and the imaginary part of vertical displacement for a vertically applied unit harmonic load, $\text{Im}[G_{33}]$, when both the source and the receiver are the same, as follows:

$$\frac{H(\omega)}{V(\omega)} = \sqrt{\frac{\text{Im}[G_{11}(\mathbf{x}, \mathbf{x}; \omega)] + \text{Im}[G_{22}(\mathbf{x}, \mathbf{x}; \omega)]}{\text{Im}[G_{33}(\mathbf{x}, \mathbf{x}; \omega)]}} \quad (8)$$

where ω denotes the circular frequency, \mathbf{x} denotes the position vectors for source and receiver which are the same, and the indices (11, 22, and 33) denote the displacement and the direction of the unit applied load, respectively (e.g., 1, north-south; 2, east-west; 3, up-down). Such calculations of the imaginary part of Green's function G in Eq. (8) are performed by the conventional discrete wavenumber summation method developed by Bouchon [20]. Then, the input data to compute H/V synthetics based on this method are the compressional and shear wave velocity, the density, the thickness, and the quality factor of each soil layer that can be retrieved in our case from GAs from the previous section. The details of the method can be found in Sánchez-Sesma et al. [18]. Equation (8) implies energy equipartition of the 3D wave field in space for a distribution of random sources. This interpretation has been revised by Kawase et al. [21] showing that the DFA approach explains well the observed H/V ratios of microtremors in Japan. Such new interpretation depends on the contribution of all waves considered in the Green's function, namely Rayleigh, Love, and body waves.

Konno and Ohmachi [3] and Bonnefoy-Claudet et al. [22] have demonstrated that the H/V curves exhibit in most cases a single peak due to the ellipticity of the fundamental mode of Rayleigh waves through 1D noise simulation; the vanishing of the vertical component occurs nearly to the fundamental resonance period of S waves where a sharp S-wave impedance contrast exists larger than 3.0 between the surface layers and the underlying stiffer formations and when the sources are near and surficial.

We calculated the observed horizontal-to-vertical spectral ratio (H/V) employing the resultant vector of the orthogonal north-south and east-west components of motion and averaging the results for all the stationary parts selected for each record (details of the digital processing of single mobile microtremors are explained [1]). To compute the synthetics' H/V ratios employing the DFA in Eq. (8), we adopted for the surface sediments above the bedrock a low-quality factor of 5.0 for all frequencies to incorporate the effects of total water saturation (since water table in POS can be found just at the surface) yielding high attenuation on wave propagation [23, 24] and a quality factor of 50 for the bedrock [25].

We present the imaginary parts of Green's functions $\text{Im}[G_{11}]$ and $\text{Im}[G_{33}]$ in **Figure 9a** and the H/V synthetics (see Eq. (8)) based on the DFA in **Figure 9b** at Queen's Park Savannah. A good agreement is found among the amplification calculations cited before for both, the fundamental period of vibration and the shape of the overall observed H/V ratios. Despite the fundamental period of 0.57 s can be explained by the ellipticity pattern depicted in **Figure 9c**, it is noted that the DFA

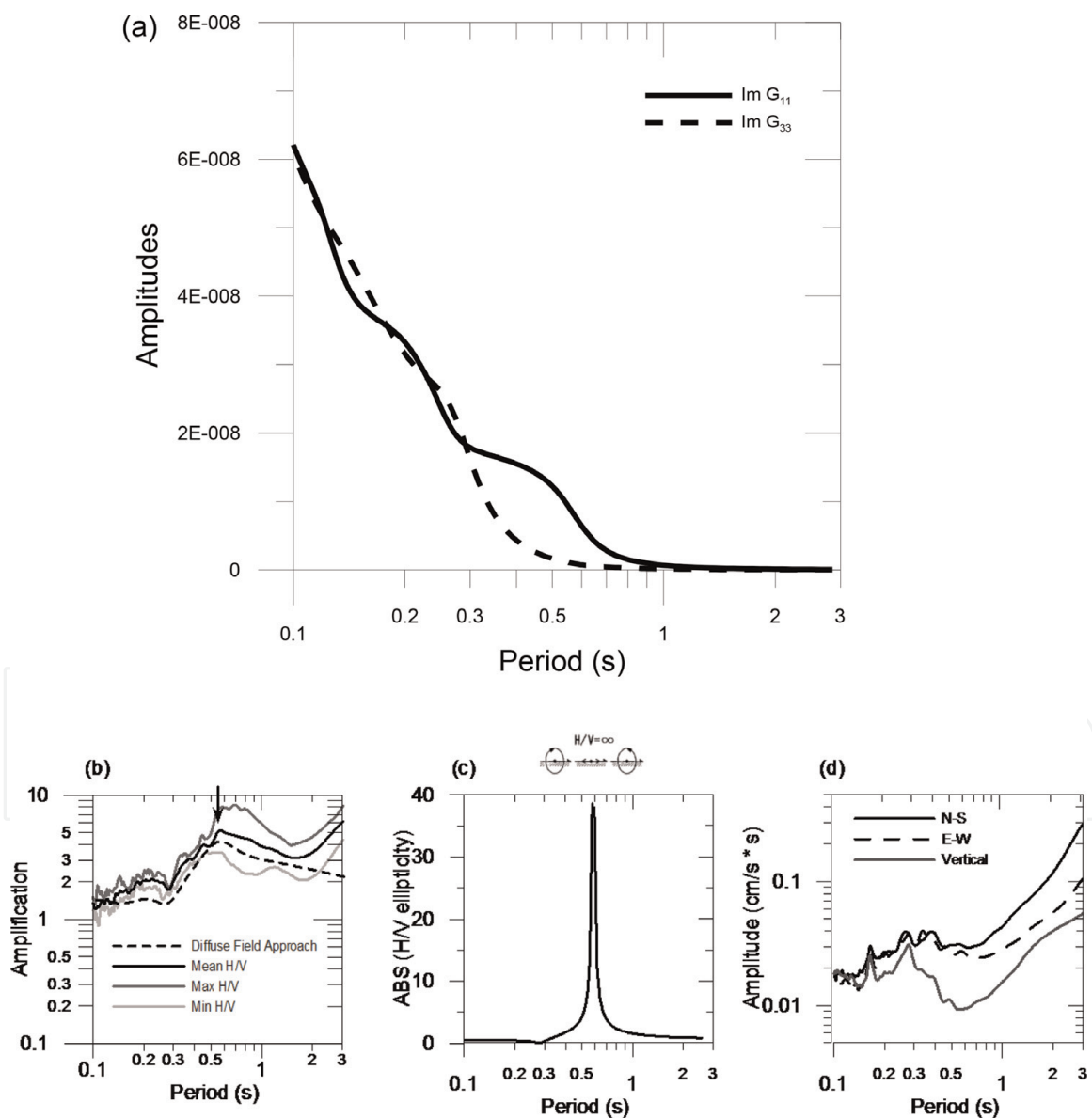


Figure 9. (a) Imaginary part of Green's function ($\text{Im} G_{11}$ and $\text{Im} G_{33}$ in Eq. (8)) via application of the Diffuse Field Approach (DFA) for Queen's Park Savanna (Point 1X in **Figure 1**); (b) H/V observed spectral ratio (mean) and H/V synthetics spectral ratios via application of DFA; (c) ellipticity of Rayleigh waves for the first mode of vibration—note that absolute values of ellipticity are drawn; and (d) absolute Fourier velocity spectrum for horizontal (N-S and E-W) and vertical components of motion. Diagram of ellipticity pattern taken from Konno and Ohmachi [3]. The fundamental period of soil T is indicated by the arrow in the H/V spectral ratios.

yields a more robust interpretation since the amplification factor cannot be measured employing the ellipticity approach.

Also, it is interesting that the change in the ellipticity pattern depicted in **Figure 9c** clearly reflects the change of particle motion from prograde to retrograde at the fundamental period of vibration observed for the theoretical and experimental calculations. The trough in the vertical component confirms the analysis causing the peak observed in the H/V ratios (**Figure 9d**).

Take the theoretical fundamental period T in seconds of a homogenous soil profile over a rigid base equal to:

$$T(s) = \frac{4H}{\bar{V}_s} \quad (9)$$

where H is the thickness of the sediments above the bedrock and \bar{V}_s is the average shear wave velocity. Introducing the values of H and V_s in Eq. (9) as 75 m and 489 m/s resulting from the GAs' inversion (Section 1.4), the period T yields 0.60s coinciding fairly well with the one obtained by the observed H/V spectral ratio technique and the one predicted by the diffuse wave field theory and the ellipticity pattern of Rayleigh waves.

The analysis for the remaining eight microtremors array sites is presented in **Figure 10**. The fundamental periods are well explained for all sites due to ellipticity pattern in the wave motion of microtremors; the DFA confirmed the effectiveness of the application of the H/V spectral technique and the GAs for the city of POS. The deeper profiles are found in the coastal areas (5X) at the Port with a total of about 225 m of sediments and a fundamental period of 1.4 s, this in accordance with water well information at the Port presented in **Table 5** that no bedrock is identified at 100 m depth. Sites in the foot of hills yield the shallower profiles of 25–30 m with fundamental periods less than 0.3 s. Intermediate periods between 0.4 and 1.0 s are found in downtown areas yielding depths between 60 and 110 m. For all array sites, V_s varies from 50 to 2000 m/s, including the bedrock.

An interesting feature of the H/V ratios can be seen for the three sites located in the coastal areas, namely, the Licensing Authority (Port Area), Mucurapo Secondary School, and Sea Lots (**Figure 10a–c**, sites 3X, 5X, and 6X, respectively, **Figure 1**). Short period components between 0.1 and 0.3 s yield a very low amplification or a de-amplification at the three sites. We attribute such phenomena due to the presence of a thin rigid layer in the surface with V_s of about 600 m/s; such feature was introduced in the search limits for the top layers in the GAs at these

Thickness (feet/m)	Description
0–7/0–2	Clay fill
7–20/2–6	Sand + gravel
20–25/6–8	Hard sand
25–110/8–34	Sand + boulders
110–115/34–35	Brown clay
115–200/35–61	Clay and boulders
200–251/61–77	Gravel with streaks of clay
251–338/77–103	Sand + boulders
	No bedrock is identified

Table 5.
Water well for the Port Area (License Office) site 5X (**Figure 1**).

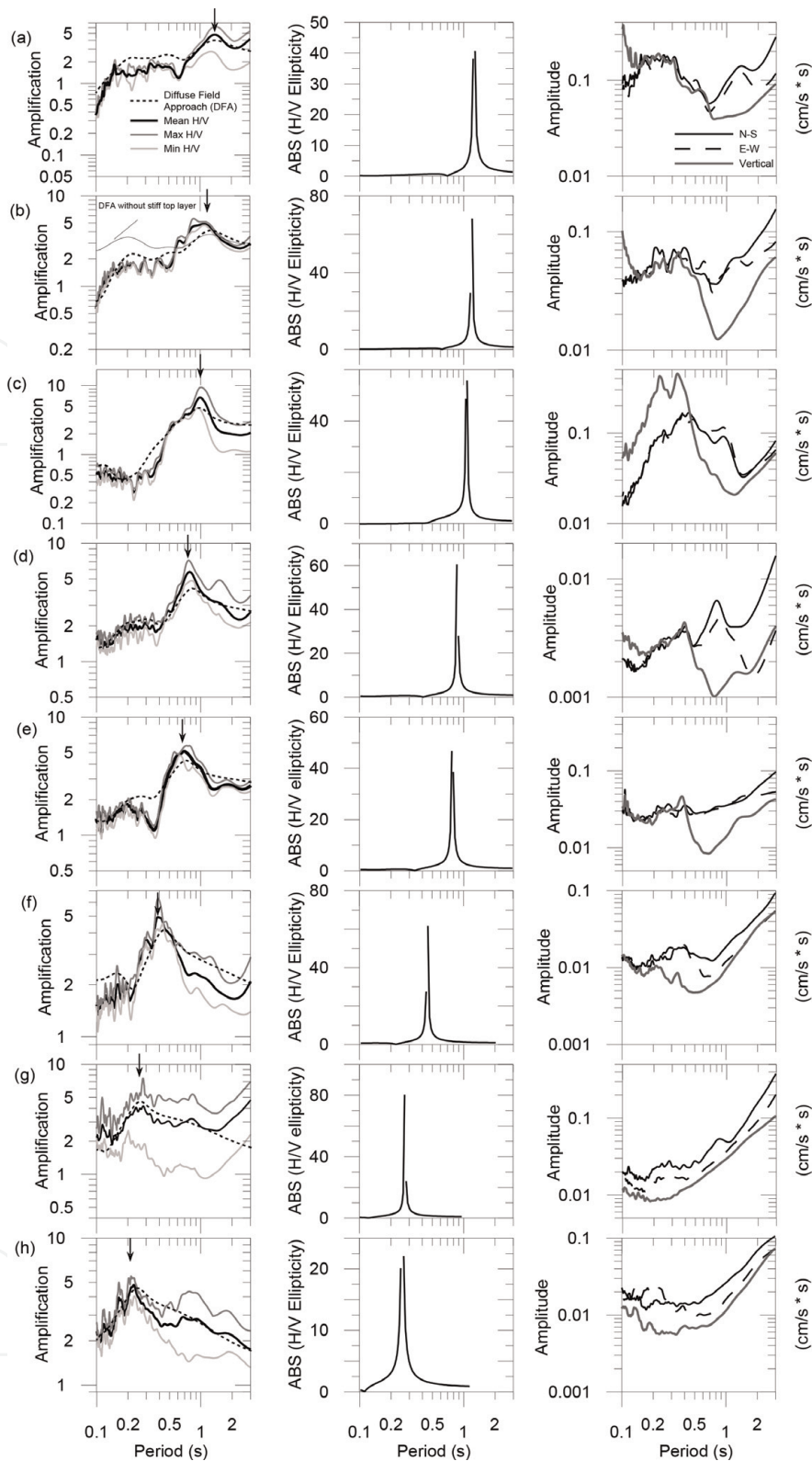


Figure 10. Left: H/V spectral ratio (observed-mean and synthetic via application of Diffuse Field Approach (DFA)). Center: ellipticity of Rayleigh waves for the first mode of vibration; note that absolute (ABS) values of ellipticity are drawn. Right: absolute Fourier velocity spectrum for horizontal (N-S and E-W) and vertical components of motion. The sites are ordered from top to bottom from the largest to the shortest fundamental period of soil T indicated by the arrows in the H/V spectral ratios. (a) Port Area (5X), (b) Mucurapo Secondary School (3X), (c) Sea Lots (8X), (d) Nelson Mandela Park (2X), (e) Woodford Square (8X), (f) Federation Park (4X), (g) St. James hospital (9X), and (h) St. Benedict's Children's home (7X). See locations of microtremors array in Figure 1.

sites. We have evidence of existing stiff layers near the surface as it is corroborated by the well logs reported by WASA near the array sites (see Hard Sand deposit in Table 5). We attribute the high V_s on the top due to compaction works, deck

constructions at the Port/Coastal Area, and/or a high degree of consolidation due to the constant presence of heavy weight (containers) that are located at these sites for shipping purposes. Note that the DFA predicted very well the H/V ratios in such circumstances as well, for both, the fundamental period and the overall shape of the transfer function. It is noted that this consolidated layer at the top of the Port Area behaves as a low pass filter and does not have an influence in the fundamental period of motion of the whole soil system; such feature was corroborated performing the DFA without the stiff top layer at Mucurapo Secondary School (see **Figure 10b**). Sea Lots site at the South East of POS (see **Figure 1** at site 6X) is characterized by the lowest V_S of 50 m/s for all array sites that correspond to a swamp area overlaid by stiff deposits. Such low values of V_S have been observed in sedimentary stratigraphy of natural intertidal flats [26].

2.2 H/V ratios and 1-D theoretical transfer function for SH-waves

Figure 11 depicts the comparison between the 1-D SH wave amplification employing the V_S profiles obtained by the GAs and the H/V observed spectral ratios. We also adopted for the surface sediments above the bedrock a low-quality

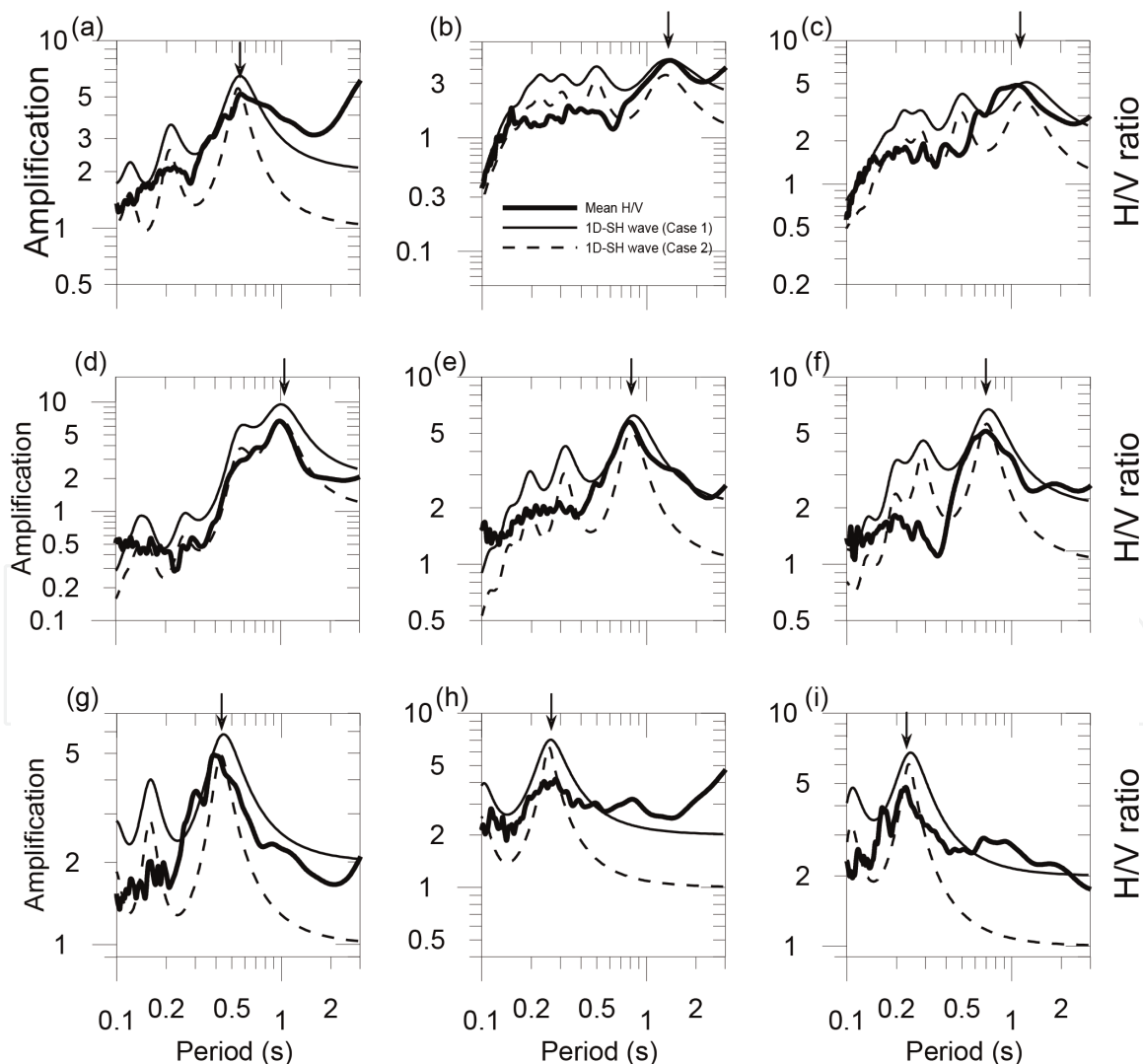


Figure 11. Comparison of H/V spectral ratios and 1-D SH wave transfer function; case (1) only up wave amplification and case (2) up + down amplification with refraction and reflection in bedrock. (a) Queen's Park Savannah array (1X), (b) Port Area (5X), (c) Mucurapo Secondary School (3X), (d) Sea Lots (8X), (e) Nelson Mandela Park (2X), (f) Woodford Square (8X), (g) Federation Park (4X), (h) St. James hospital (9X), and (i) St. Benedict's Children's home (7X). The fundamental period of soil T is indicated by the arrows.

factor of 5.0 for all frequencies to incorporate the effects of total water saturation. We plotted two kinds of theoretical SH transfer functions, namely, case (1) up + down amplification with refraction and reflection in bedrock and case (2) only up wave amplification. In both cases the 1-D SH wave amplification replicates the fundamental period of the observed H/V ratios; however, in most of the cases, the overall shape of the H/V ratios differs mainly at long period components for case (1) and for short period components for case (2). It is noticed that a level of amplification yield between three and five yields at the predominant peak. This level of amplification is referred to the bedrock motion.

3. V_{S30} and fundamental period

An important parameter in the modification of seismic waves propagating toward the surface is the composition of the near-surface soil layers. In different building codes around the world, the average shear wave velocity of the upper 30 m (V_{S30}) has been adopted to characterize the response of seismic waves to the influence of near-surface strata.

In first instance, we compared the V_{S30} obtained from our microtremors array observation and the ones estimated by the empirical formulas of Matsuoka et al. [27] employing 2000 sites in Japan based on geomorphological units.

We calculated the V_{S30} from our microtremor results using the following formula:

$$V_{S30} = \frac{30}{\sum_{i=1}^N \frac{h_i}{V_i}} \quad (10)$$

where h_i and V_i denote the thickness (in meters) and the shear wave velocity of the i th layer; N is the total number of soil layers respectively.

We classified the sites (1X–5X, 8X) as a Gravelly Terrace, Sea Lots (site 6X) as a Reclaimed Land, and St. Dominic's Children's Home to the East (7X) and St. James Hospital to the West (9X) as Mountain Foot Slope sites (see **Figure 1**). The empirical formulas to estimate V_{S30} (m/s) for the Gravelly Terrace (Eq. (11)), the Reclaimed Land (Eq. (12)), and the Mountain Foot Slope (Eq. (13)) yield:

$$\log VS30 = 2.493 + 0.072\log Ev + 0.027\log Sp - 0.164\log Dm \pm 0.122(\sigma) \quad (11)$$

$$\log VS30 = 2.373 - 0.124\log Dm \pm 0.123(\sigma) \quad (12)$$

$$\log VS30 = 2.602 \pm 0.092(\sigma) \quad (13)$$

where Ev is the elevation (m), Sp refers to the Tangent of Slope*1000, Dm yields the distance (km) from mountain or hill, and σ denotes the standard deviation. We took Dm as the shortest distance to the Northern Range or the Laventille Metalimestone foothills (**Figure 1**). The results are presented in **Figure 12**. In general the estimated V_{S30} from the empirical formulas of Matsuoka et al. [27] estimates well the velocities obtained by the GA's from our array measurements in the range of $\pm\sigma$ (standard deviation). We also compared the V_{S30} of our microtremors array profiles with the ones estimated by Allen and Wald [28] using the topographic slope as a proxy of site conditions employing the USGS Web Server (earthquake.usgs.gov/hazards/apps/vs30/). We retrieved the correspondent predicted V_{S30} at the location of each microtremors array. The most noticeable difference is observed for the mountain foot slope in St. James (site 9X). However, we did not find a good correlation when comparing with soil types proposed by

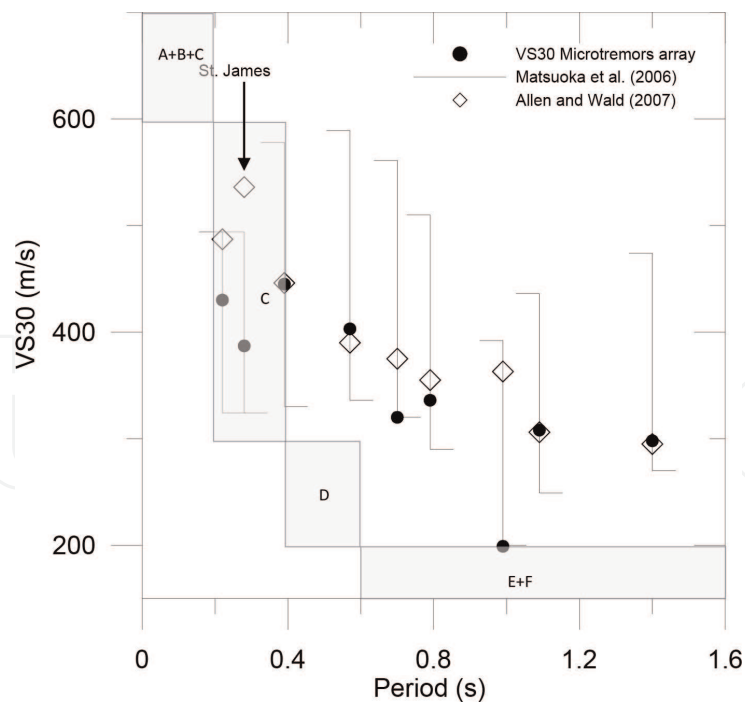


Figure 12. Comparison of VS30 (m/s) retrieved from our microtremors array and the empirical formulas of Matsuoka [27] and the method of Allen and Wald [28]. The shadowed area represents the classification of Zhao and Xu [29] based on fundamental period of soil and VS30.

Zhao and Xu [29] based on NEHRP classes on VS30 (shadowed areas in **Figure 12**). This leads to suggest to characterize the soil at POS by the fundamental period rather than the VS30 [30]; Zhao and Xu [29] suggest also that site period is a better parameter for characterizing soil conditions, in very deep or very soft sediments.

4. Preliminary assessment of liquefaction susceptibility

Nakamura [31] proposed a technique to investigate the liquefaction susceptibility based on microtremor measurements, namely, the vulnerability index K_g for the surface ground, as follows:

$$K_g = \frac{A_g^2}{F_g} \quad (14)$$

where A_g is the amplification factor referenced to the engineering bedrock and F_g is the predominant frequency of vibration of the soil profile (the inverse of the period); both values can be taken from the horizontal-to-vertical spectral ratio (H/V) of microtremors; A_g is considered to be the H/V ratio at the predominant frequency. Values of K_g greater than 20 are considered likely to liquefy. The authors computed the liquefaction potential using Eq. (14) at each point and develop an iso-liquefaction potential map interpolating the K_g value of the 1181 single mobile microtremors data employed in Salazar et al. [1] (**Figure 13**). The results are very concerning regarding this hazard because the water table in POS can be found just at the surface, the soil conditions then are saturated sands and gravels, and sometimes poorly consolidated reclaimed land has been placed specially in the coastal areas. The areas with a high liquefaction susceptibility are The Port, Sea Lots, some parts of Woodbrook, a small spot in Cocorite (where in fact reclaimed land exists), and some small areas in the Queen's Park Savannah and Federation Park. Also South

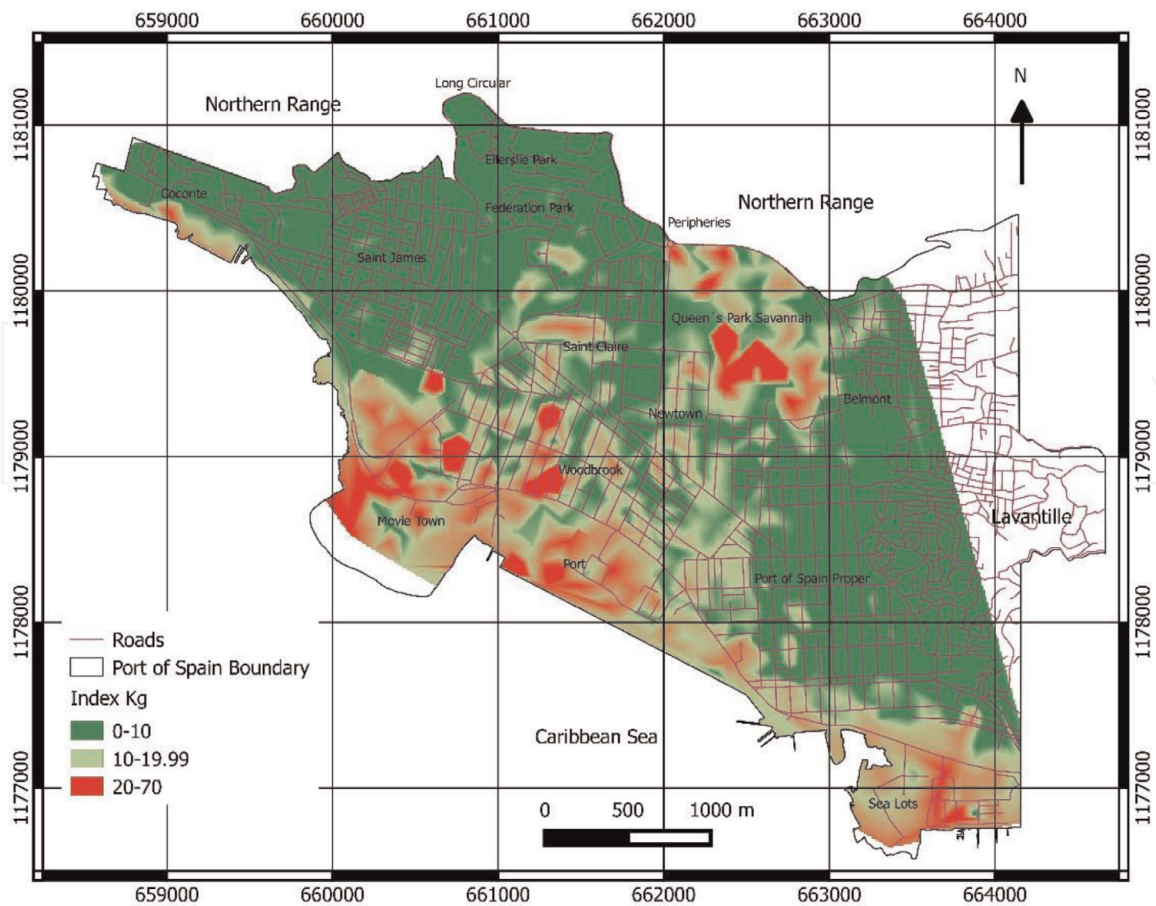


Figure 13. Preliminary liquefaction hazard map for Port of Spain City, employing Nakamura index K_g (see Eq. (14)). Zones yielding a K_g above 20 are suggested to a high liquefaction susceptibility.

of Saint James in the Coastal area yields a possibility of high liquefaction potential. Evidence of soil subsidence is already present in some structures near the Port Area as the Lighting House Tower (**Figure 14**). Next to it, the Eric Williams Complex known as the Twin Towers which are one of the tallest buildings in POS (92 m height) has been constructed in the 1980s incorporating piles on their foundations; the eyewitness during the construction process affirmed that some piles sank totally during their driving process due to extremely soft soil conditions found at that time in the coastal area. Several new high-rise buildings including hotels, a water front, high-income class dwellings, amenity centers, and the Port itself are located in this high liquefaction susceptibility area. Ironically, Sea Lots located to the West is characterized by a very low-income social class; it is also a prone area of high potential of liquefaction. It is noted that the study of Kraft [32] employing the methodology of Holzer et al. [33] yielded similar conclusions for POS and another cities of Trinidad employing regional geological map conditions.

5. Conclusions

Shear wave velocity V_S profiles were determined by performing nine microtremors array surveys in Port of Spain (POS), Trinidad, employing the spatial autocorrelation SPAC method and genetic algorithms (GAs); the results yielded V_S between 50 and 2000 m/s at POS. The ellipticity pattern for the first mode of Rayleigh waves explains the resulting predominant peak in the H/V Nakamura ratios for all array sites. We validated the soil profiles retrieved by the SPAC and GAs' schemes comparing the synthetics' horizontal-to-vertical spectral (H/V) ratios



Figure 14. *Leaning lighthouse tower at the Port Area. See the displacement Δ at the top of the structure due to the soil subsidence at its foundation.*

generated by the Diffuse Field Approach (DFA) with the observed ones at the array sites and with empirical formulas to estimate the average shear wave velocity of the upper 30 m (V_{S30}). We conclude that the H/V ratios yield a genuine shear wave fundamental period of vibration of the soil profiles at POS, and that can be used to validate the high-resolution seismic microzonation map proposed by Salazar et al. [1]. The amplification and fundamental period of motion retrieved from the microtremors together with the water table level suggest a high liquefaction potential mainly on the coastal areas. It looks that in terms of seismic amplification and liquefaction hazard, a safe place is the Laventille area at the East characterized geologically by a metalimestone; unfortunately it is classified with the highest crime rate and drug dealers in Trinidad.

The genetic inversion results revealed that the deeper parts of POS are located in the Port Area and South of Woodbrook with a depth of 225 m and the softer materials are located at the South East of POS in Sea Lots with low V_S of 50 m/s which correspond to a buried swamp or mangrove; toward the north of the City, the depth of the sediments decreases substantially from 75 m in the Savannah to 30 m in Saint James and Cocorite to the West. Toward the South East part of POS in Sea

Lots, the depth of sediments yields 80 m. Generally, the V_S in the sediments increases with depth in the range mainly of 50 m/s to 600 m/s, and the variants of the stiffness in the soil are mainly found near the surface due to the reclaimed land—compacted or not—during construction works or the presence of swampy soil to the East of POS. We have also corroborated via successive rounds of genetic inversions that the V_S at the bedrock yields 2000 m/s.

It is worth mentioning that the DFA even reproduced the whole shape of the H/V ratios, including peaks and troughs and the level of amplification; such characteristics cannot be retrieved employing the Rayleigh wave pattern interpretation. It seems that the H/V spectral ratio technique from Nakamura represents a true piece of information regarding the dynamic properties of the sediments above bedrock in terms of identification of the fundamental period of the soil profile when comparing with the one retrieved with the 1-D SH wave theoretical amplification as well; it is noticed that an amplification level yields between three and five at the fundamental period. However, the H/V spectral ratios do not coincide with the whole shape of the 1-D SH transfer function. If we proved just incorporating the fundamental mode in the phase velocity inversion that our resonant peak in the H/V ratios is genuine, then we did not incorporate higher modes in the inversion; however, future research lines on this topic would allow us to introduce the first overtones in new analysis [34]. The V_{S30} retrieved from our microtremors array coincides well with the predicted V_{S30} of Matsuoka et al. [27] when incorporating geomorphological conditions; however, we did not find a good correlation with NEHRP classification on V_{S30} [29] suggesting that the fundamental period is a superior parameter for classification than the V_{S30} in this case.

Borehole data in POS reaching the bedrock is very limited, and a parallel research would be focused on conducting boreholes reaching the depth of the bedrock at new strong motion stations or critical facilities, and if possible, to get the V_S employing alternative methods (e.g., cross hole or laboratory soil test); borehole data would help to validate the proposed preliminary liquefaction hazard map and can be used to implement remedial measures against such hazard, especially at the coastal port area. The last hazard peer-reviewed maps for Trinidad and the Eastern Caribbean have been proposed by Bozzoni et al. [35] yielding 0.60 g of peak ground acceleration for POS setting 2475 years return period at a rock site class B in NEHRP classification; such shaking level is strong enough to trigger the liquefaction in the saturated alluvium at POS.

Since our microtremor survey only permits to study the soil behavior in the linear range, the effect of the non-linearity in the soil is still a big question to solve for the area. Future research lines might be focused on a frequency-dependent quality factor as well.

Acknowledgements

The authors thank IntechOpen for inviting us to write a chapter of this book and editor John Tiefenbacher for his sincere and fruitful comments during the revision process.

The microtremor recordings were provided by the Ministry of Planning and Sustainable Development of Trinidad and Tobago and are proprietary.

We used QGIS Open Software version 2.4 and the GCC Fortran Compiler to generate the maps presented in this work. The V_{S30} values used in this work were retrieved via WEB server at USGS (earthquake.usgs.gov/hazards/apps/vs30/) last accessed January 9, 2016.

The authors thank the Ministry of Planning and Sustainable Development of Trinidad and Tobago for funding this research being conceived by the first author as a principal investigator while working at the Seismic Research Centre in Trinidad

during 2008–2014. We thank also all the governmental institutions in Trinidad that permit to do the survey in their facilities. We greatly acknowledge Hiroaki Yamanaka (Tokyo Institute of Technology) for providing the first author the original Fortran Codes of Genetic Inversion through the sponsor of the Japanese International Cooperation Agency (JICA) in El Salvador. The Tokyo Sokushin personnel in Japan were always assisting us with our queries regarding the microtremor instrumentation. The authors want to thank Francisco Sánchez-Sesma from Universidad Autónoma de México UNAM for sharing with the first author the Diffuse Field Approach program to compute the synthetics of H/V ratio. His unconditional help has made possible to update this chapter to better understand the amplification phenomena employing microtremor measurements at Port of Spain.

Author details


Walter Salazar^{1*}, Garth Mannette², Kafele Reddock² and Clevon Ash²

1 Faculty of Engineering and Architecture, Catholic University of El Salvador (UNICAES), El Salvador

2 Seismic Research Centre, The University of the West Indies (UWI), St. Augustine, Trinidad and Tobago

*Address all correspondence to: walter.salazar@catolica.edu.sv

IntechOpen

© 2019 The Author(s). Licensee IntechOpen. This chapter is distributed under the terms of the Creative Commons Attribution License (<http://creativecommons.org/licenses/by/3.0>), which permits unrestricted use, distribution, and reproduction in any medium, provided the original work is properly cited. 

References

- [1] Salazar W, Mannette G, Reddock K, Ash C. High-resolution grid of H/V spectral ratios and spatial variability on microtremors at Port of Spain, Trinidad. *Journal of Seismology*. 2017;**21**:1541-1557. DOI: 10.1007/s 10950-017-9681-1
- [2] Crichlow M. Groundwater Recharge in the Queen's Park Savannah. Trinidad: The Water Resource Agency of Trinidad and Tobago WASA; 1989
- [3] Konno K, Ohmachi T. Ground-motion characteristics estimated from spectral ratio between horizontal and vertical components of microtremors. *Bulletin of the Seismological Society of America*. 1998;**88**:228-241
- [4] Nakamura Y. A method for dynamic characteristics estimation of subsurface using microtremor on the ground surface. Quick Report of the Railway Research Institute. 1989;**30**(1):25-33
- [5] Aki K. Space and time spectra of stationary stochastic waves, with special reference to microtremors. *Bulletin of the Earthquake Research Institute*. 1957; **35**:415-457
- [6] Okada H. The Microtremor Survey Method. The Society of Exploration Geophysicist. Oklahoma: Tulsa; 2003. 135 pp
- [7] Miyakoshi K, Okada H, Suqun S. A range of wavelengths to estimate the phase velocities of surface waves in microtremors. In: Proc. 94th SEG T Conf. 1996. pp. 178-182 (in Japanese)
- [8] Yamanaka H, Ishida H. Application of genetic algorithms to an inversion of surface-wave dispersion data. *Bulletin of the Seismological Society of America*. 1996;**86**:436-444
- [9] Haskell NA. The dispersion of surface waves on multi-layered media. *Bulletin of the Seismological Society of America*. 1953;**43**:17-34
- [10] Scherbaum F, Hinzen K, Ohrnberger M. Determination of shallow shear wave velocity profiles in the Cologne, Germany area using ambient vibration. *Geophysical Journal International*. 2003;**152**:597-612
- [11] Schmitz M, Alvarado L, Lüth S. The velocity structure of the Cariaco sedimentary basin, northeastern Venezuela, from the refraction seismic data and possible relation to earthquake hazard. *Journal of South American Sciences*. 2005;**18**(2):89-105
- [12] Kitzunezaki CNG, Kobayashi Y, Ikawa T, Horike M, Saito T, Kurota T, et al. Estimation of P- and S-wave velocity in deep soil sediments for evaluating ground vibrations in earthquake. *Journal of Japan Society for Natural Disaster Science*. 1990;**9**(3):1-17 (in Japanese)
- [13] Karagoz O, Chimoto K, Citak S, Ozel O, Yamanaka H, Hatayama K. Estimation of S-wave velocity structure and site response characteristics by microtremors array measurements in Tekirdag region, NW Turkey. *Earth, Planets and Space*. 2015;**67**:176
- [14] Lomax A, Snieder R. Finding sets of acceptable solutions with a genetic algorithm with application to surface wave group dispersion in Europe. *Geophysical Research Letters*. 1994;**21**: 2617-2620. DOI: 10.1029/94GL02635
- [15] Ólafsdóttir EA. Multichannel Analysis of Surface Waves, Methods for Dispersion Analysis of Surface Wave Data. Reykjavík: University of Iceland, School of Engineering and Natural Sciences; 2014. p. 70
- [16] Arai H, Tokimatsu K. S-wave velocity profiling by joint inversion of

microtremor dispersion curve and horizontal-to-vertical (H/V) spectrum. *Bulletin of the Seismological Society of America*. 2005;**95**(5):1766-1778

[17] Sánchez-Sesma F, Pérez-Ruiz A, Luzón F, Campillo M, Rodríguez-Castellanos A. Diffuse fields in dynamic elasticity. *Wave Motion*. 2008;**45**: 641-654

[18] Sánchez-Sesma F, Rodríguez M, Iturrarán-Viveros U, Luzón F, Campillo M, Margein L, et al. A theory for microtremors H/V spectral ratio: Application for a layered medium. *Geophysical Journal of International Banner. Express Letter*. 2011;**186**(1): 221-225

[19] Perton M, Sánchez-Sesma FJ, Rodríguez-Castellanos A, Campillo M, Weaver R. Two perspectives on equipartition in diffuse elastic fields in three dimension. *Journal of the Acoustical Society of America*. 2009;**126** (3):1125-1130

[20] Bouchon M. A simple method to calculate Green's functions for elastic layered media. *Bulletin of the Seismological Society of America*. 1981; **71**(4):959-971

[21] Kawase H, Matsushima S, Satoh T, Sánchez-Sesma F. Applicability of theoretical-to-vertical ratio of microtremors based on the diffuse field concept to previously observed data. *Bulletin of the Seismological Society of America*. 2015;**105**(6):3092-3103

[22] Bonnefoy-Claudet S, Cornou C, Bard P, Cotton F, Moczo P, Kristek J, et al. H/V ratio: A tool for site effects evaluation. Results from 1-D noise simulations. *Geophysical Journal International*. 2006;**167**:827-837

[23] Bodin P, Horton S. Broadband microtremor observation of basin resonance in the Mississippi

embayment, central us. *Geophysical Research Letters*. 1999;**26**(7):903-906

[24] Crane JM. Effects of stress and water saturation on seismic velocity and attenuation in near surface sediments [doctor philosophy dissertation]. USA: Mississippi College; 2013. p. 146

[25] Campbell K. Estimates of shear-wave Q and κ_0 for unconsolidated and semiconsolidated sediments in eastern North America. *Bulletin of the Seismological Society of America*. 2009; **99**(4):2365-2392

[26] Watabe Y, Sassa S. Sedimentary stratigraphy of natural intertidal flats with various characteristics. *Soils and Foundations*. 2012;**52**(3):411-429

[27] Matsuoka M, Wakamatsu K, Fujimoto K, Midorikawa S. Average shear wave velocity mapping using Japan engineering geomorphologic classification map. *Structural Engineering/Earthquake Engineering*. 2006;**23**(1):57s-68s

[28] Allen T, Wald D. Topographic Slope as a Proxy for Seismic Site-Conditions (V_{s30}) and Amplification Around the globe. Open-File Report 2007-1357. Reston, Virginia: U.S. Geological Survey; 2007

[29] Zhao J, Xu H. A comparison of V_{s30} and site period as site-effect parameters in response spectral ground-motion prediction equation. *Bulletin of the Seismological Society of America*. 2013; **103**:1-18

[30] McVerry G. Site-effect as continuous functions of site period and V_{s30} . In: Proceedings of the Ninth Pacific Conference on Earthquake Engineering, Building and Earthquake-Resilient Society; 14-16 April; Auckland, New Zealand. 2011

[31] Nakamura Y. Seismic vulnerability indices for ground and structures using

microtremors. In: World Conference on Railway Research, Florence. 1997

[32] Kraft J. Development of liquefaction susceptibility and hazard maps for the Islands of Jamaica and Trinidad [master thesis]. USA: Georgia Institute of Technology; 2013. p. 109

[33] Holzer TL, Noce TE, Bennett MJ. Liquefaction probability curves for surficial geologic deposits. *Environmental and Engineering Geoscience*. 2011;**17**(1):1-21

[34] Rivet D, Campillo M, Sánchez-Sesma F, Shapiro N, Singh K. Identification of surface wave higher modes using a methodology based on seismic noise and coda waves. *Geophysical Journal International*. 2015; **203**:856-868

[35] Bozzoni F, Corigliano M, Lai C, Salazar W, Scandella L, Zuccolo E, et al. Probabilistic seismic hazard assessment at the eastern Caribbean Islands. *Bulletin of the Seismological Society of America*. 2011;**101**(5):2499-2521